Electronic Supplementary Material (ESI) for Journal of Materials Chemistry A.
This journal is © The Royal Society of Chemistry 2022

# Supplemental Information

## Co/Li-dual-site Doping Enables $LiCoO_2$ as High-voltage, Fast-charging, and Long-cycling Cathode Material

Shou-Xiao Chen,[a] Chuan-Wei Wang,[a] Yao Zhou,[a] Jun-Ke Liu,[a] Chen-Guang Shi,[b] Guo-Zhen Wei,[c] Bao-Yi Yin,[d] Hao-Tian Deng,[a] Si-Yu Pan,[a] Ming-Jia Guo,[b] Wei-Chen Zheng,[b] Hao-Zhi Wang,[e] You-Hong Jiang,[b] Ling Huang,[b] Hong-Gang Liao,[b] Jun-Tao Li[a,*], and Shi-Gang Sun[b]

### Methods

*Pristine $LiCoO_2$ material synthesis:* The $Co_3O_4$ precursor powder was synthesized by a co-precipitation method. $CoSO_4 \cdot 7H_2O$ (1405.75 g, AR, 99%, Aladdin) was dissolved in deionized water. The above solution, NaOH aqueous solution (10 M), and ammonia water ($NH_3 \cdot H_2O$, 3 M) were pumped into a batch reactor (25 L) containing deionized water gradually to control the PH to 11. During the reaction, a protective gas of nitrogen ($N_2$) must be continuously added to remove oxygen ($O_2$) in the reactor at 50 $^oC$. The precursor is obtained through multiple washing, suction filtration, and drying in a vacuum oven for 24 hours at 110 $^oC$. To generate the $LiCoO_2$, the obtained precursor and $LiOH \cdot H_2O$ (AR, 99%, Aladdin) were mixed uniformly according to the stoichiometric ratio and then sintered at 1,000 $^oC$ for 6 hours under flowing $O_2$. Identically, the Al-doped $Co_3O_4$ powder precursor powder was synthesized by a co-precipitation method. $CoSO_4 \cdot 7H_2O$ (1405.75 g, AR, 99%, Aladdin) and $Al_2(SO_4)_3$ (17.12 g, 99.95%, Aladdin) were dissolved in deionized water. This mixed solution, the solution of sodium hydroxide (NaOH, 10 M), and ammonia water ($NH_3 \cdot H_2O$, 3 M) were

pumped into a batch reactor (25 L) containing deionized water gradually to control the PH to 11. During the reaction, a protective gas of nitrogen ($N_2$) must be continuously added to remove oxygen ($O_2$) in the reactor at 50 $^oC$. The precursor is obtained through multiple washing, suction filtration, and drying in a vacuum oven for 24 hours at 110 $^oC$. To generate the A-LCO, the obtained precursor and $LiOH·H_2O$ (AR, 99%, Aladdin) were mixed uniformly according to the stoichiometric ratio and then sintered at 1,000 $^oC$ for 6 hours under flowing $O_2$.

*$Nb_{18}W_{16}O_{93}$ material synthesis:* The $Nb_{18}W_{16}O_{93}$ materials were prepared by a solid-state reaction method, a mixture of $Nb_2O_5$ and $WO_3$ was thoroughly ground in an agate mortar for 2 hours and then transferred to a star ball milling for 6 hours. Next, the homogeneous mixture was calcined at 1,200 $^oC$ for 12 hours. The prepared $Nb_{18}W_{16}O_{93}$ particles are processed into nano-scale particles in a pulverizer.

*ANW-LCO material synthesis:* The nanosized $Nb_{18}W_{16}O_{93}$ fine particles are coated on A-LCO particles (NWO@LCO) with a mass ratio of 2 wt% (NWO: LCO) through a high-speed solid-phase coating machine (NOBILTA−130, Hosokawa Micron). Then, through high-temperature annealing at a gradient temperature (450 $^oC$, 550 $^oC$, and 650 $^oC$), NWO reacts with LCO, niobium element (Nb), and tungsten element (W) are uniformly sintered into the bulk phase of $LiCoO_2$ to obtain the final products which are named ANW-LCO-450, ANW-LCO-550, and ANW-LCO-650.

*Half-cell assembly:* Eighty wt% active material, 10 wt% super-p as the conductive material, and 10 wt% polyvinylidene fluoride (PVDF, 99.5%, Aladdin) as a binder were

in N-methyl pyrrolidone (NMP) to form a slurry as the active cathode. Then, the mixed slurry, after ball milling, was evenly coated on the carbon-coated aluminum foil. After the aluminum foil is completely dried in a 40 $^{o}$C blast drying oven, and the aluminum foil is transferred to a vacuum drying oven at 100 $^{o}$C for 12 hours, and then cut to prepare a lithium cobalt oxide positive electrode for the lithium-ion battery. It is cut to prepare cathode plates for $LiCoO_2$ with an active material loading of 5−6 mg $cm^{-2}$. Half-cell assembly used 2025 type-cope with lithium metal as an anode, the electrolyte was 1.0 mol $L^{-1}$ $LiPF_6$ in EC: EMC (= 3:7 by volume) with 10 wt% FEC as additive. The assembly of sulfide-based all-solid-state lithium-ion batteries (ASSLIBs) is composed of lithium indium alloy as the anode, $Li_{10}GeP_2S_{12}$ (LGPS) as the solid electrolyte, and LCO as the cathode. Each active cathode was homogenized with LCO, LGPS, and acetylene black and at a weight ratio of 60:38:2.

*Electrochemical tests:* The galvanostatic current charge and discharge test of the half-cell is carried out in the voltage range of 2.7−4.4 V, 2.7−4.5 V, and 2.7−4.6 V (versus $Li/Li^+$) on LAND-2001A battery tester (Wuhan, China) at room temperature. The rate performance tests were performed at a current density of 0.1 C, 0.5 C, 1 C, 2 C, 5 C, 10 C, 15 C and finally back to 0.1 C (1 C=180 mA $g^{-1}$) at 4.5 V (versus $Li/Li^+$). The cycle performance test was performed at a current density of 0.5 C under 4.5 V and 4.6 V (versus $Li/Li^+$) after activation at 0.1 C, and the long cycle performance were performed at a current density of 10 C under 4.5 V and 15 C at 4.4 V (versus $Li/Li^+$) after activation at 0.1 C. Both the Cyclic Voltammetry (CV) test at a rate of 0.1, 0.3,

0.5, and 0.7 mV $s^{-1}$ in a voltage range of 2.7−4.5 V (versus Li/$Li^+$) and the electrochemical impedance spectroscopy (EIS) test (100 kHz−0.1 Hz) were performed on the CHI 660D electrochemical workstation purchased from Shanghai, China.

*Materials characterizations:* The crystal structure, phase structure, and evolution analysis of the material are characterized by ex-situ X-ray diffractometer [XRD, Rigaku Ultima IV, Cu Kα radiation (λ = 1.5406 Å), 40 kV, 40 Ma] and the in-situ XRD patterns were detected on an in-situ X-ray diffractometer (Bruker D8 discover) at a current density of 0.5 C when the cells were cycling in the potential range of 2.7−4.5 V. The field emission scanning electron microscope (FESEM, Hitachi S-4800) at 10 kV probed SEM images of all prepared samples. To further observe the microstructure and morphology of the material, we used a high-resolution transmission electron microscope (F20) to obtain a TEM slices image. TEM slices were acquired by cryo-microtome (Leica EM UC7FC7). X-ray chemical analysis electron spectroscopy microprobe (XPS, Quantum 2000) was carried out obtaining the surface and a certain depth element analysis of the cathode material. The element distribution on the surface and cross-section of the material were obtained by electron probe microanalysis (EPMA, JXA8530F, JEOL Co.) We used an ion beam cutter (Leica EM TIC3X) to obtain the cross-section of the material. In situ DEMS measurements were conducted on a homemade electrochemical flow cell which held a specially designed coin cell (2.7−4.5 V). The cell setup was connected to a mass spectrometer which monitored the $O_2$ and $CO_2$ evolution status when the cell was charged.

*DFT calculations:* All the calculations were performed within the framework of the density functional theory (DFT) as implemented in the Vienna Ab initio Software Package (VASP 5.3.5) code within the Perdew–Burke–Ernzerhof (PBE) generalized gradient approximation and the projected augmented wave (PAW) method.[1] The cutoff energy for the plane-wave basis set was set to 450 eV. The convergence criterion for the electronic self-consistent iteration and force was set to $10^{-5}$ eV and 0.01 eV/Å, respectively. The Brillouin zone of the surface unit cell was sampled by Monkhorst–Pack (MP) grids.[2] The $LiCoO_2$ bulk and p (3×3) $LiCoO_2$ (001) were determined by 8×8×2 and 4×4×1 Monkhorst−Pack grid. A vacuum layer of 15 Å was introduced to avoid interactions between periodic images. The PBE+U approach was applied to calculations of the electronic structure of $LiCoO_2$ which can partly reduce the underestimation of the electronic bandgap and the excessive tendency to delocalize the electron density. In this work, we set the Hubbard parameter to U-J = 5 eV for Co, which ensures a good qualitative description of the structure and electronic properties of materials. The climbing image nudged elastic band (CI-NEB) method was used to confirm the transition states with only one imaginary frequency along with the reaction coordinates.[3]

**Supplementary Figure**

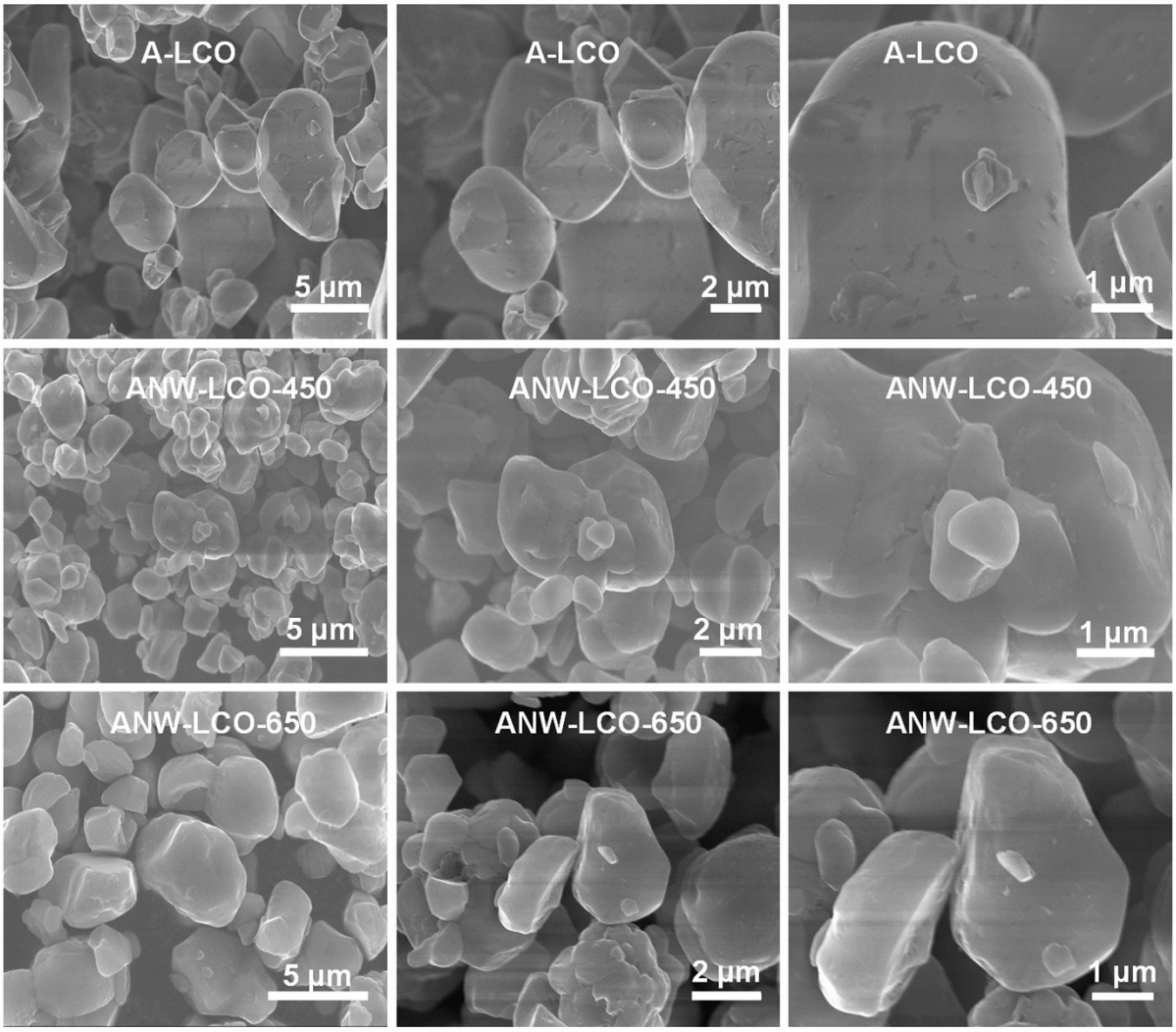


**Figure S1.** SEM images of A-LCO, ANW-LCO-450, and ANW-LCO-650.

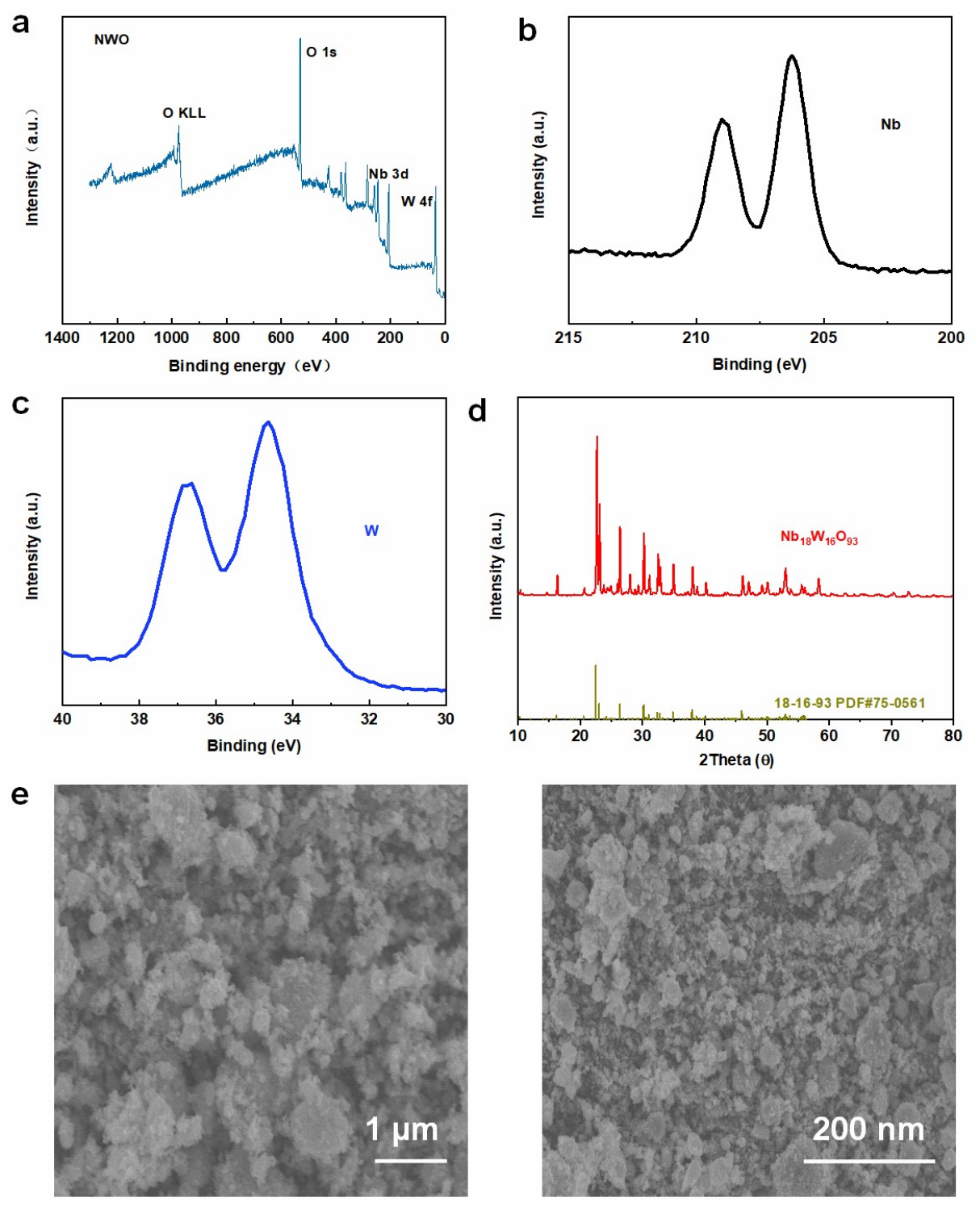


**Figure S2. a.** X-ray spectroscopy (XPS) patterns of $Nb_{18}W_{16}O_{93}$. **b.** Nb 3d XPS spectrum of ANW-LCO-550. **c.** W 4f XPS spectra of ANW-LCO-550. **d.** XRD patterns of $Nb_{18}W_{16}O_{93}$. **e.** SEM images of $Nb_{18}W_{16}O_{93}$.

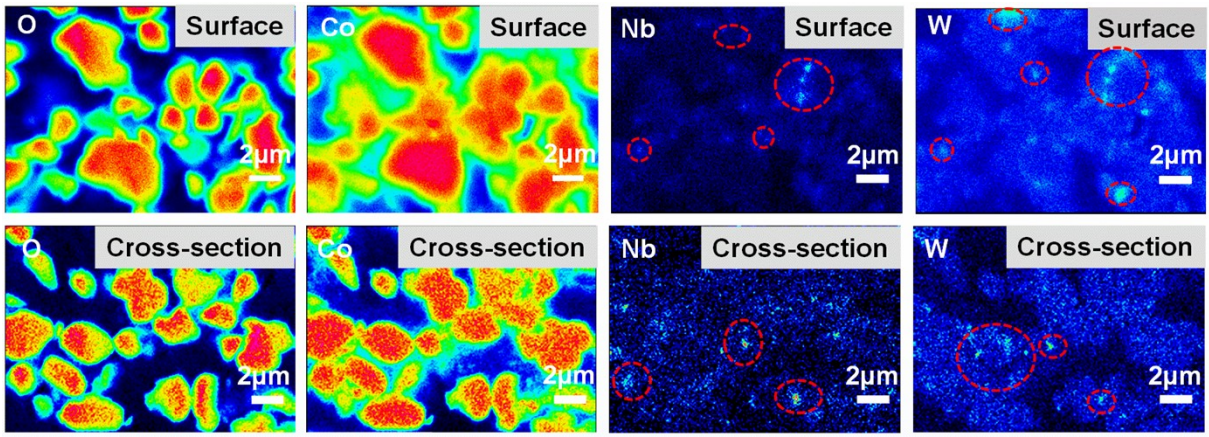


**Figure S3.** Electron probe micro-analyzer mapping images of b) surface-section and c) cross-section of ANW-LCO-550. Detection elements: O, Co, Nb, and W, respectively.

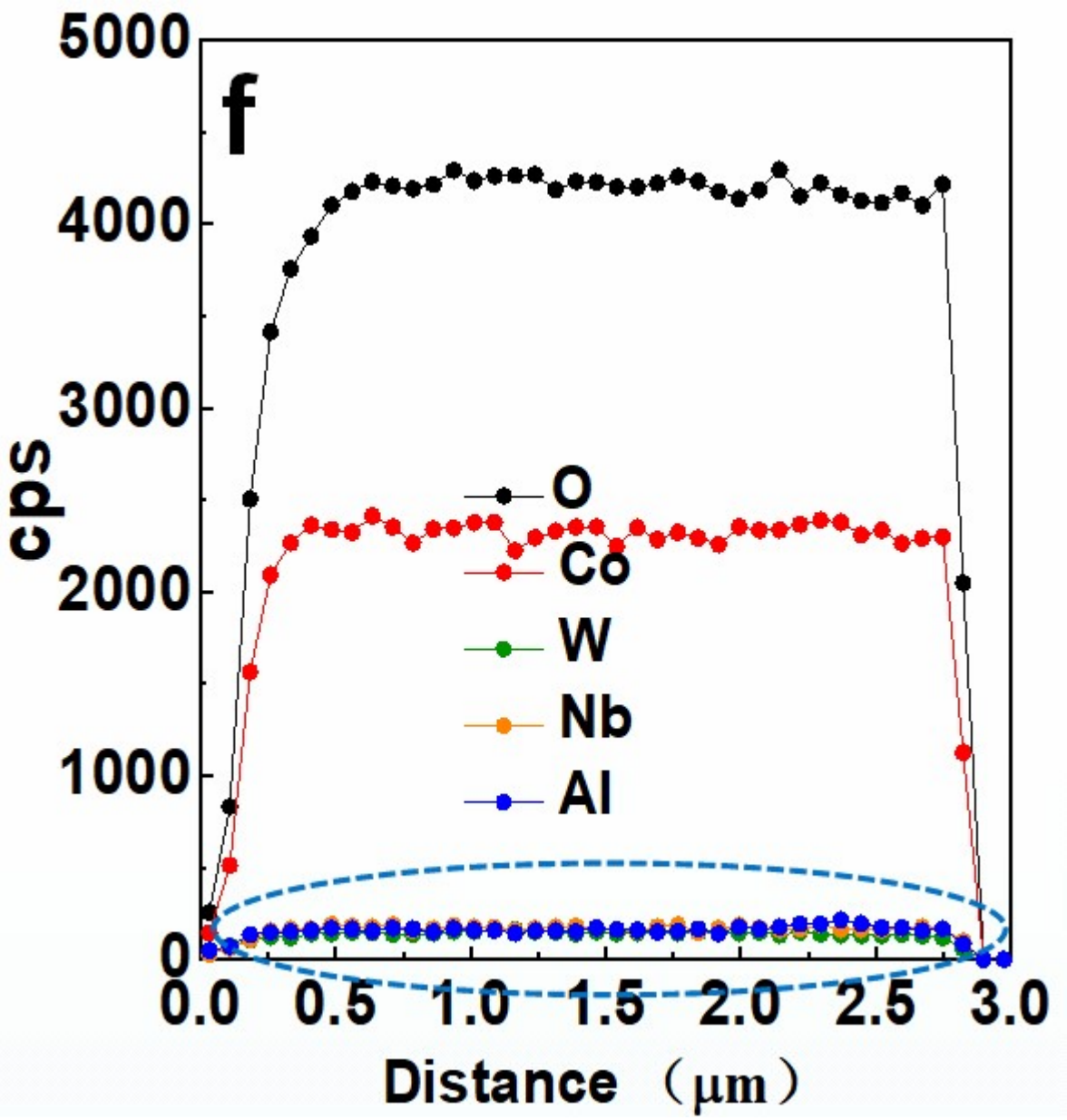


**Figure S4.** Counting intensity (cps) of ANW-LCO-550 from EDS.

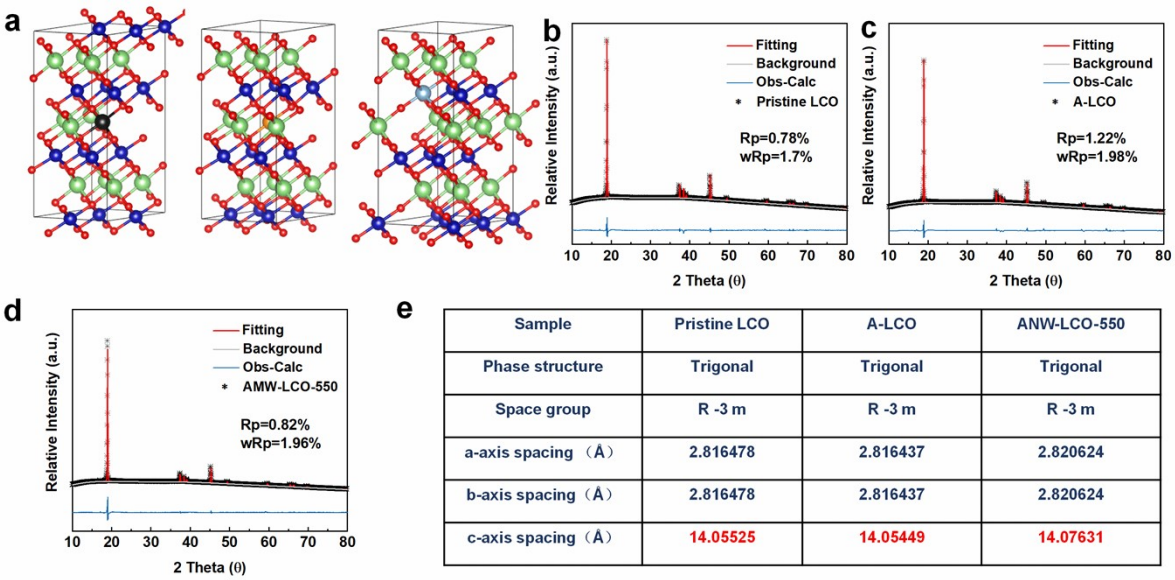


e

| Sample | Pristine LCO | A-LCO | ANW-LCO-550 |
|---|---|---|---|
| Phase structure | Trigonal | Trigonal | Trigonal |
| Space group | R -3 m | R -3 m | R -3 m |
| a-axis spacing（Å） | 2.816478 | 2.816437 | 2.820624 |
| b-axis spacing（Å） | 2.816478 | 2.816437 | 2.820624 |
| c-axis spacing（Å） | 14.05525 | 14.05449 | 14.07631 |

**Figure S5. a.** Schematic diagram of the structure after Al, Nb, and W directly replace different sites of LCO. **b−d.** Ex-situ XRD characterization and structural refinement of **b.** Pristine LCO, **c.** A-LCO, and **d.** ANW-LCO-550. **e.** The phase structure, space group, and lattice parameters were obtained by structural refinements of pristine LCO, A-LCO, and ANW-LCO-550.

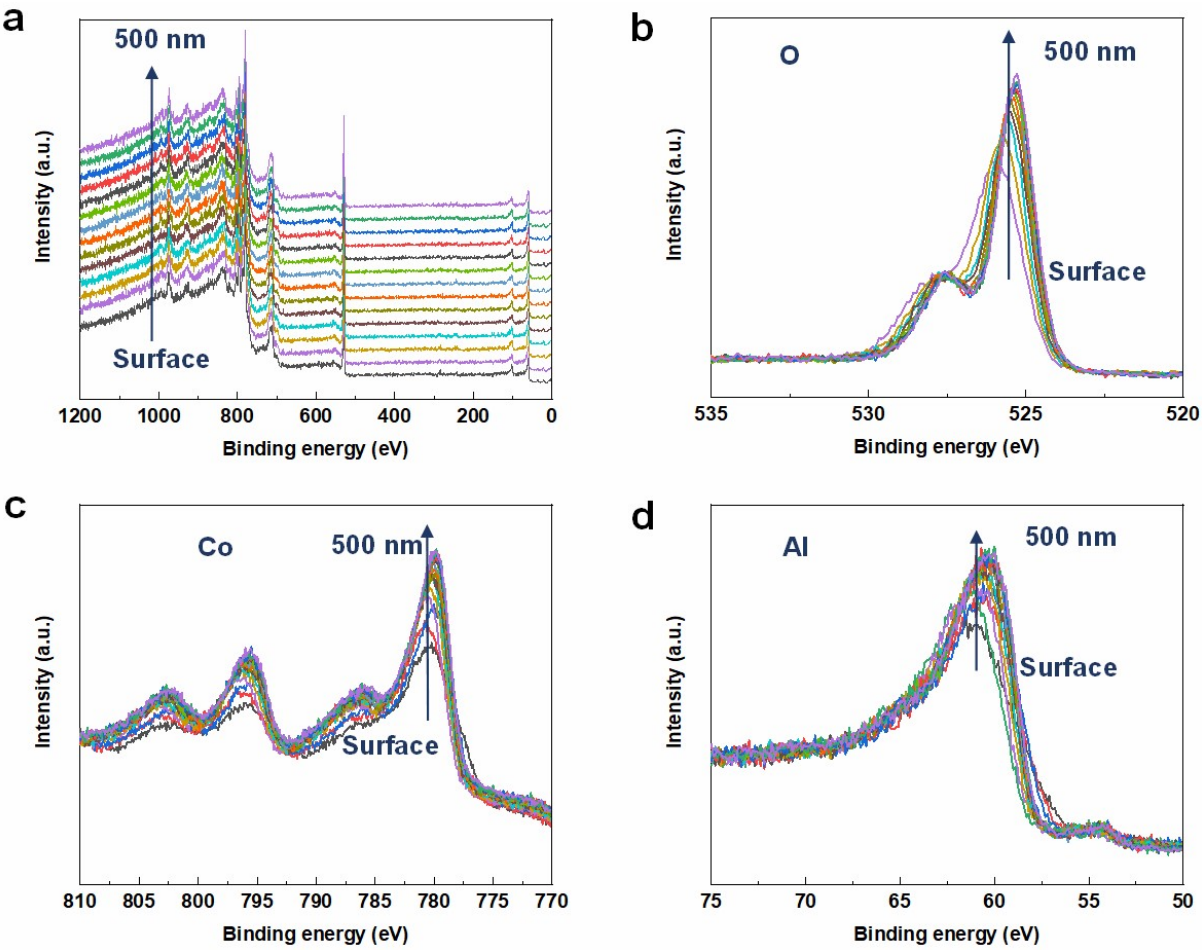

**Figure S6. a.** The in-depth profiles XPS spectra of ANW-LCO-550 (0 nm-500 nm). **b.** Al 2p, **c.** Co 2p, and **d.** O 1s XPS spectra of ANW-LCO-550.

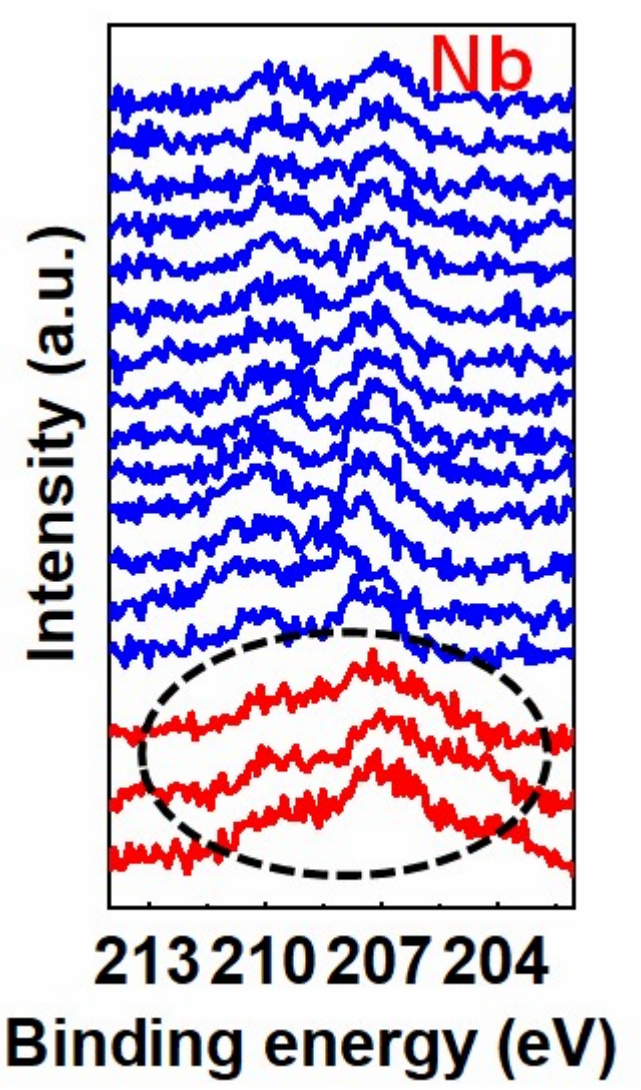


**Figure S7.** The in-depth Nb 3d XPS spectra of ANW-LCO-550.

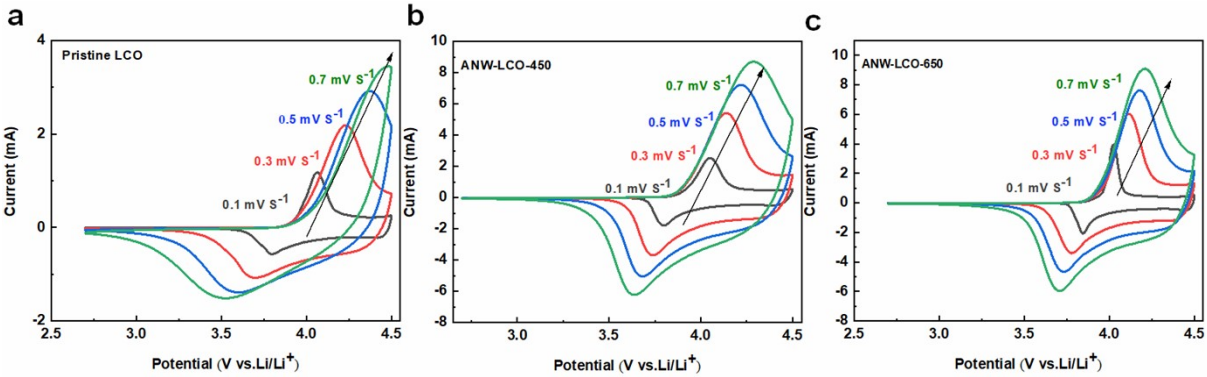

**Figure S8.** Cyclic voltammograms (CV) were obtained under various sweeping rates (0.1 mV $s^{-1}$, 0.3 mV $s^{-1}$, 0.5 mV $s^{-1}$, and 0.7 mV $s^{-1}$) of pristine LCO, ANW-LCO-450, and ANW-LCO-650.

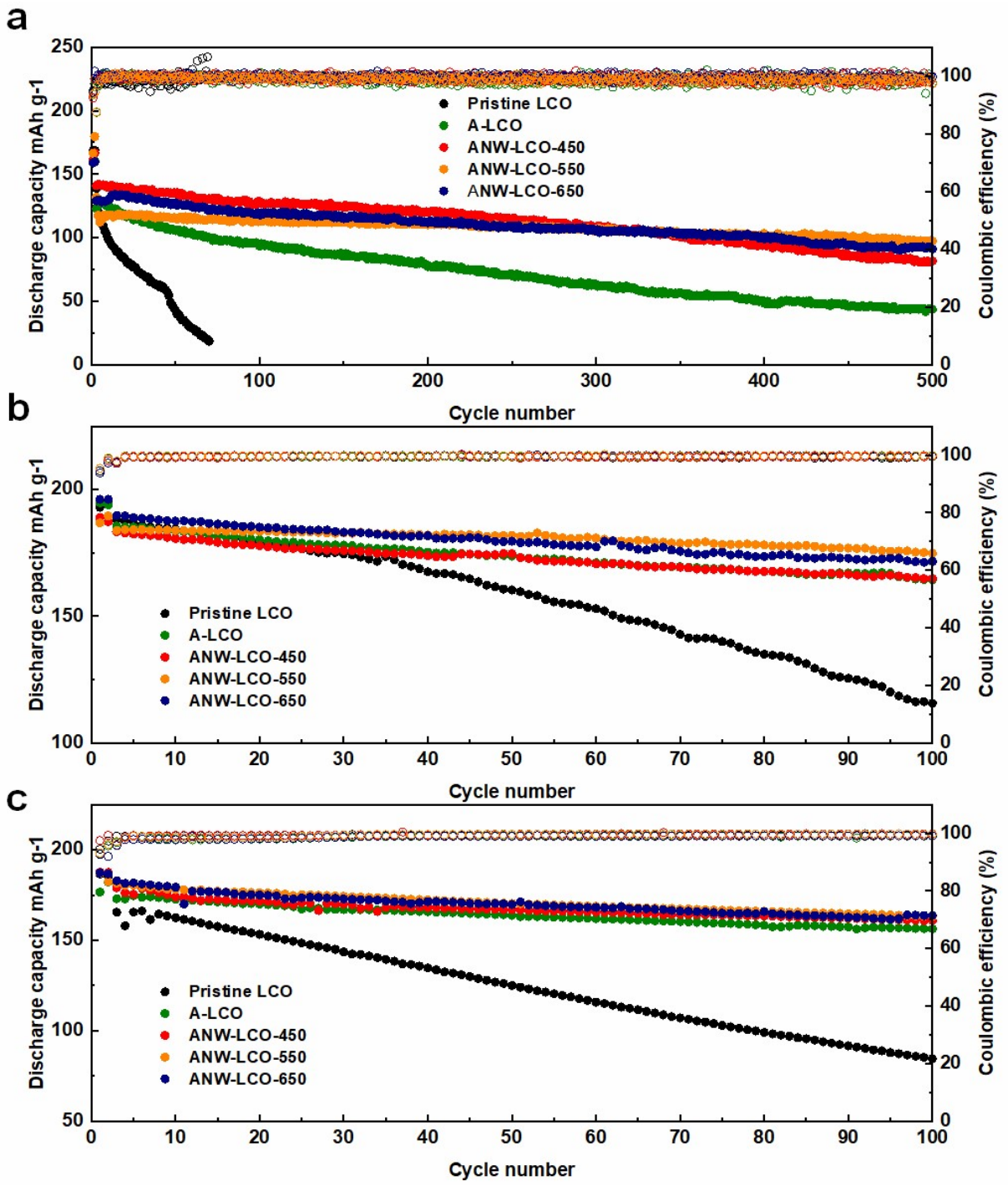


**Figure S9. a.** Long cycling (500 cycles) performance at the current density of 15 C (1 C=180 mA $g^{-1}$), the cells were cycled at the range of the voltage 2.7–4.4 V (25 $^{o}$C). **b.** Long cycling (100 cycles) performance at the current density of 0.5 C (1 C=180 mA $g^{-1}$), the cells were cycled at the range of the voltage 2.7-4.5 V (25 $^{o}$C). **c.** Long cycling

(100 cycles) performance at the current density of 0.5 C (1 C=180 mA $g^{-1}$), the cells were cycled at the range of the voltage 2.7 –4.5 V (50 °C).

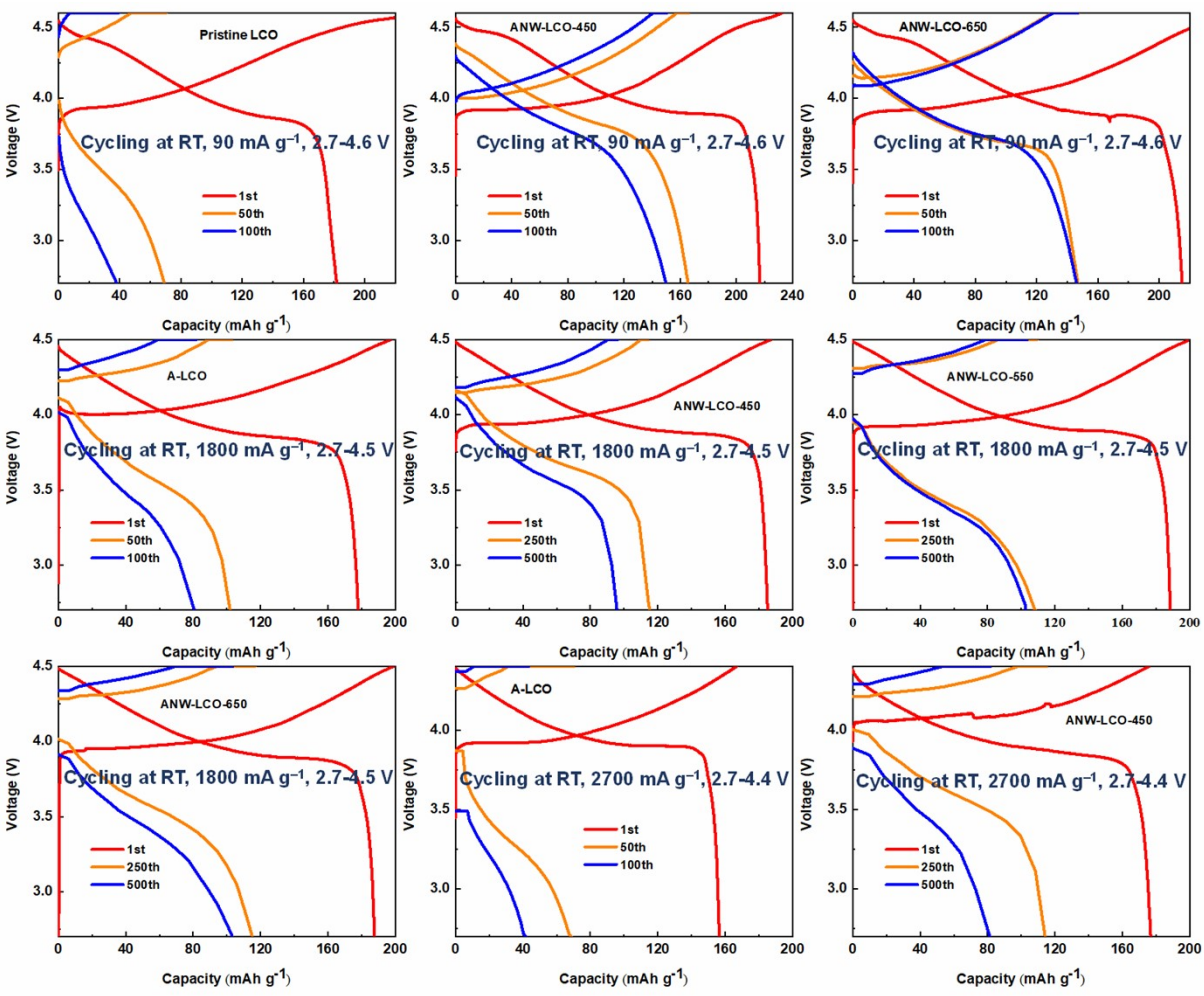

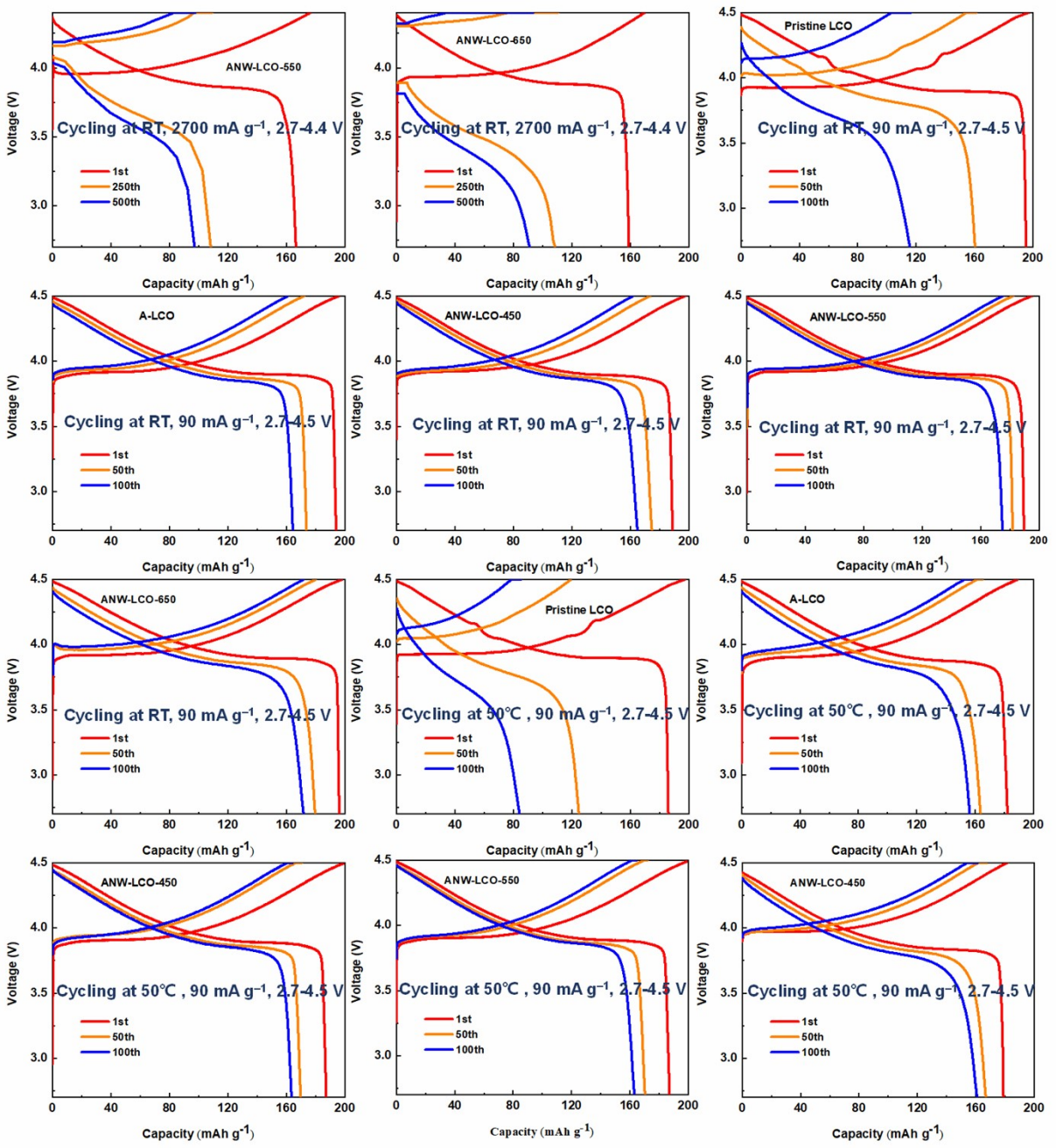


**Figure S10.** The charge-discharge curves after different cycles of different cathodes.

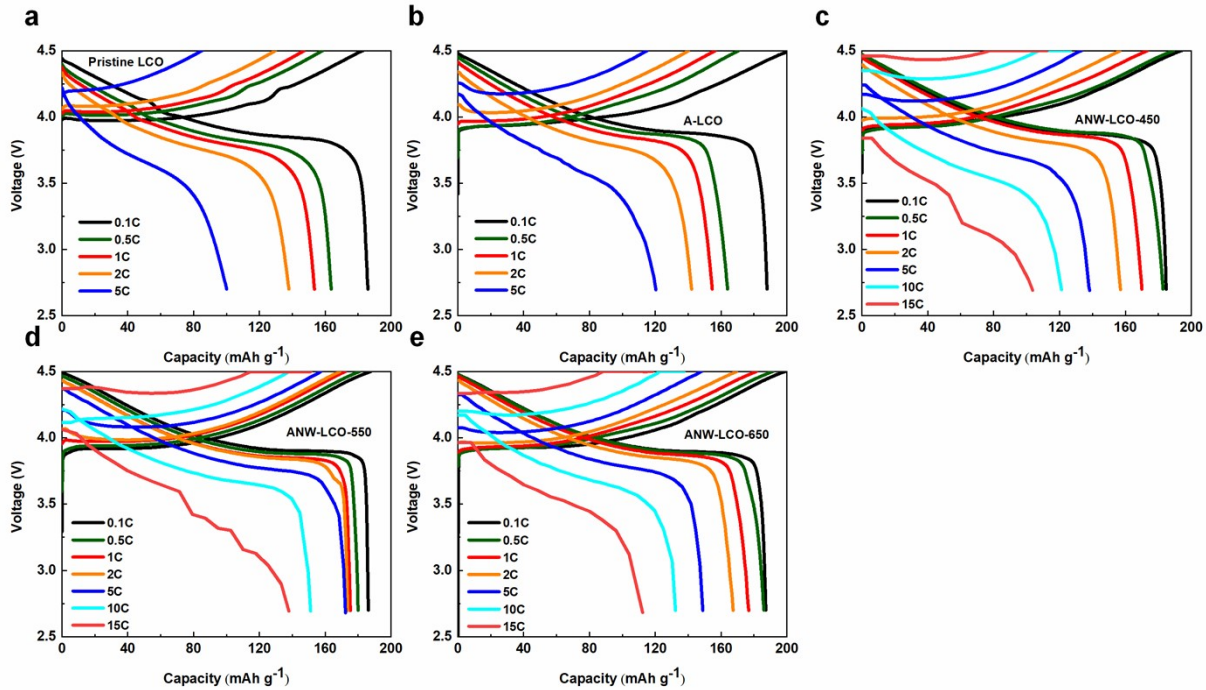


**Figure S11.** The charge-discharge curves at 0.1 C, 0.5 C, 1 C, 2 C, and 5 C of **a.** Pristine LCO. The charge-discharge curves at 0.1 C, 0.5 C, 1 C, 2 C, 5 C, and 10 C of **b.** A-LCO. The charge-discharge curves at 0.1 C, 0.5 C, 1 C, 2 C, 5 C, 10 C, and 15 C of **c.** ANW-LCO-550, **d.** ANW-LCO-550, and **e** ANW-LCO-650.

**Table S1.** Summary of the electrochemical performances of $LiCoO_2$|Li half-cell.

| Condition | Sample | Cycle number | Rate (C) (1 C = 180 mA $g^{-1}$) | Residual capacity (mAh g-1) | Capacity retention (%) | CE (%) (first cycle) | CE (%) average |
|---|---|---|---|---|---|---|---|
| 2.7−4.5 V, 25 °C | Pristine LCO | 100 | 0.5 | 115.7 | 61.44 | 94.52 | 99.39 |
| | A-LCO | 100 | 0.5 | 164.4 | 88.58 | 95.42 | 99.45 |
| | ANW-LCO-450 | 100 | 0.5 | 164.9 | 89.91 | 95.39 | 99.42 |
| | ANW-LCO-550 | 100 | 0.5 | 174.9 | 95.11 | 93.81 | 99.77 |
| | ANW-LCO-650 | 100 | 0.5 | 171.7 | 90.46 | 95.42 | 99.76 |
| 2.7−4.5 V, 50 °C | Pristine LCO | 100 | 0.5 | 84.5 | 51.06 | 94.5 | 99.21 |
| | A-LCO | 100 | 0.5 | 156.3 | 90.35 | 93 | 98.87 |
| | ANW-LCO-450 | 100 | 0.5 | 160.9 | 89.88 | 97.5 | 99.56 |
| | ANW-LCO-550 | 100 | 0.5 | 163.2 | 89.87 | 92.7 | 98.80 |
| | ANW-LCO-650 | 100 | 0.5 | 163.7 | 89.5 | 93.2 | 99.36 |
| 2.7−4.6 V, 25 °C | Pristine LCO | 100 | 0.5 | 38.1 | 25.88 | 92 | 97.54 |

| | | | | | | | |
|---|---|---|---|---|---|---|---|
| | A-LCO | 100 | 0.5 | 99.6 | 56.66 | 91.26 | 99.43 |
| | ANW-LCO-450 | 100 | 0.5 | 146.2 | 75.09 | 92 | 99.43 |
| | ANW-LCO-550 | 100 | 0.5 | 150.9 | 77.92 | 92.27 | 99.5 |
| | ANW-LCO-650 | 100 | 0.5 | 145 | 77.50 | 91.38 | 99.47 |
| 2.7−4.4 V, 25 °C | Pristine LCO | 70 | 15 | / | / | 94.77 | / |
| | A-LCO | 500 | 15 | 43.4 | 35.4 | 93.77 | 98.77 |
| | ANW-LCO-450 | 500 | 15 | 81.6 | 57.55 | 92.45 | 99.31 |
| | NWO-LCO-550 °C | 500 | 15 | 97.4 | 73.9 | 94.4 | 99.64 |
| | ANW-LCO-650 | 500 | 15 | 91 | 70.54 | 93.61 | 99.05 |
| 2.7−4.5V, 25 °C | Pristine LCO | 70 | 10 | / | / | 98 | / |
| | A-LCO | 632 | 10 | / | / | 94.01 | / |
| | ANW-LCO-450 | 1000 | 10 | 68.5 | 41.29 | 93.2 | 99.93 |
| | NWO-LCO-550 °C | 1000 | 10 | 85.3 | 60.36 | 94.01 | 99.4 |
| | ANW-LCO-650 | 1000 | 10 | 66.2 | 41.43 | 92.86 | 99.27 |

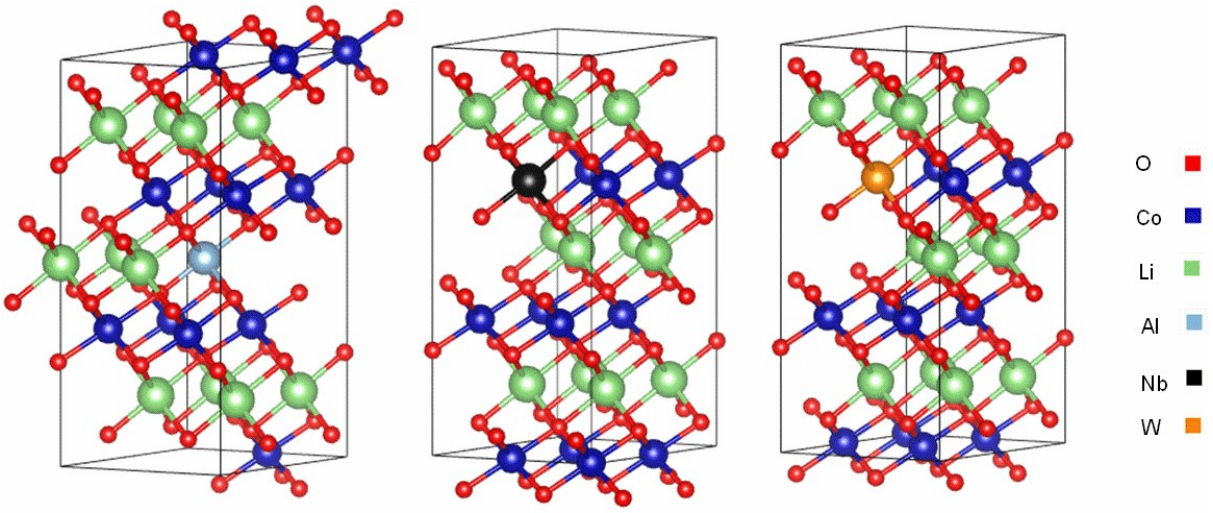


| Sample | Pristine LCO | Al-Li-1 ($Al_{Li}^{\cdot\cdot}$) | Nb-Co-2 ($Nb_{Co}^{\cdot\cdot}$) | W-Co-2 ($W_{Co}^{\cdot\cdot\cdot}$) |
|---|---|---|---|---|
| a-axis spacing (Å) | 2.81 | 2.83 | 2.82 | 2.83 |
| b-axis spacing (Å) | 2.81 | 2.82 | 2.83 | 2.83 |
| c-axis spacing (Å) | 13.91 | 13.84 | 14.01 | 14.00 |
| Volume ($Å^3$) | 95.00 | 95.64 | 96.95 | 96.85 |

**Figure S12.** The calculation model and lattice parameters obtained by DFT.

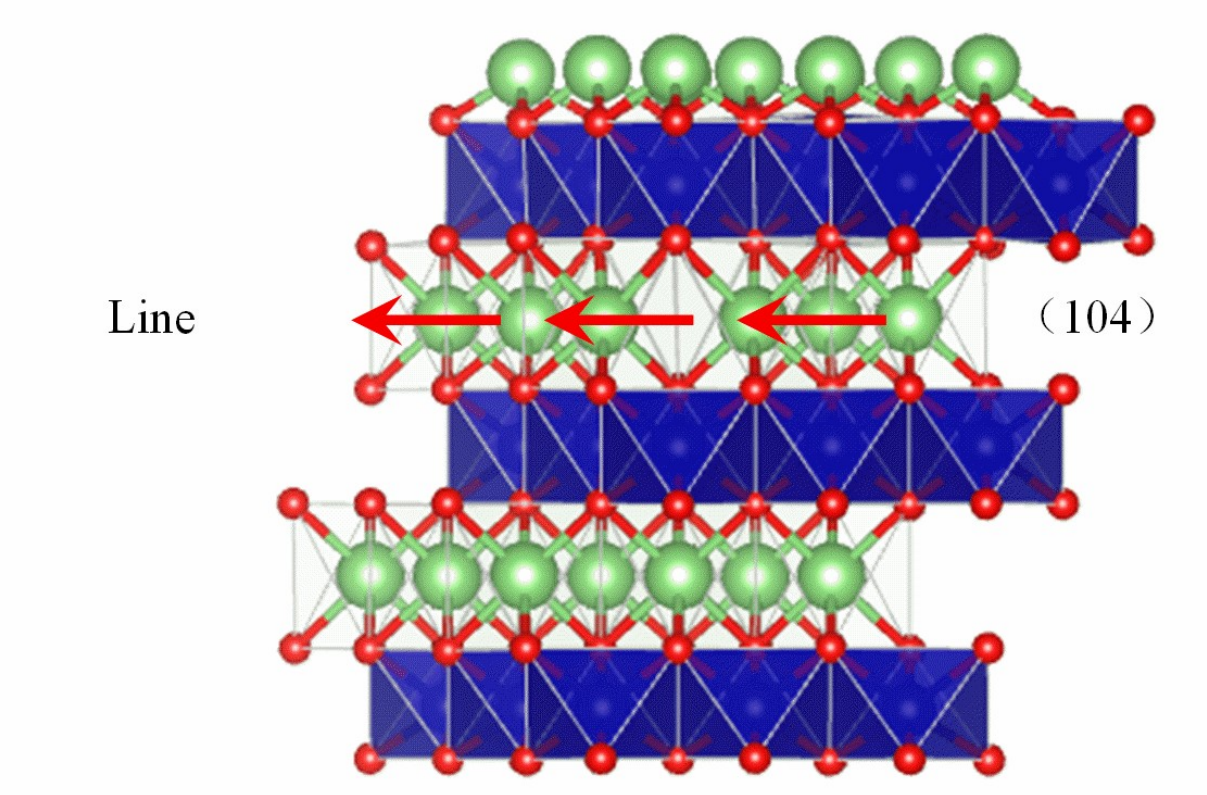


**Figure S13.** Schematic diagram of the $Li^+$ transmission channel of LCO on (104).

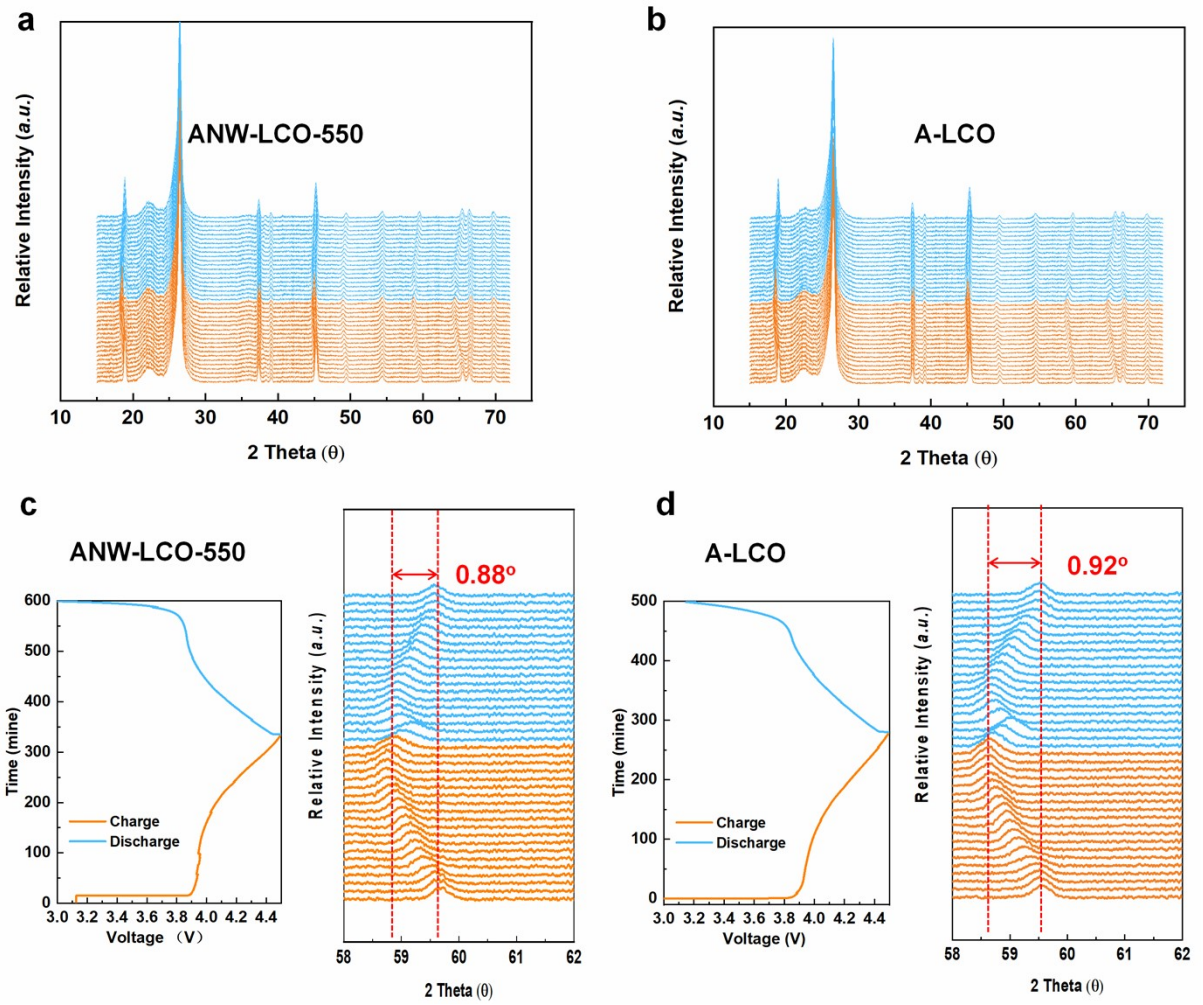


**Figure S14. a-b.** In-situ XRD characterization for **a.** ANW-LCO-550 and **b.** A-LCO during the first charge-discharge process. **c-d.** The evolution of the (107) peak of **c.** ANW-LCO-550 and **d.** A-LCO.

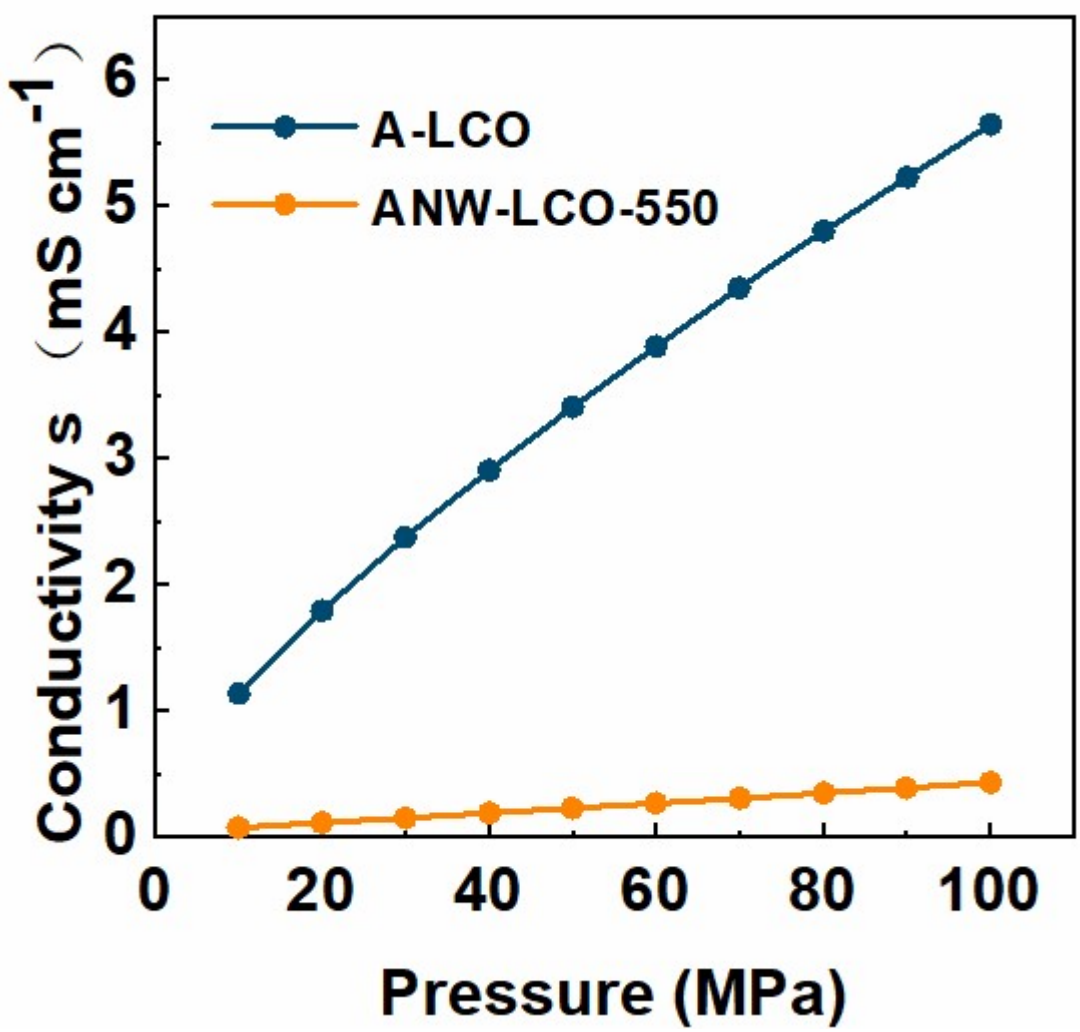


**Figure S15.** The electronic conductivity of the A-LCO and ANW-LCO-550 from the two-electrode method.

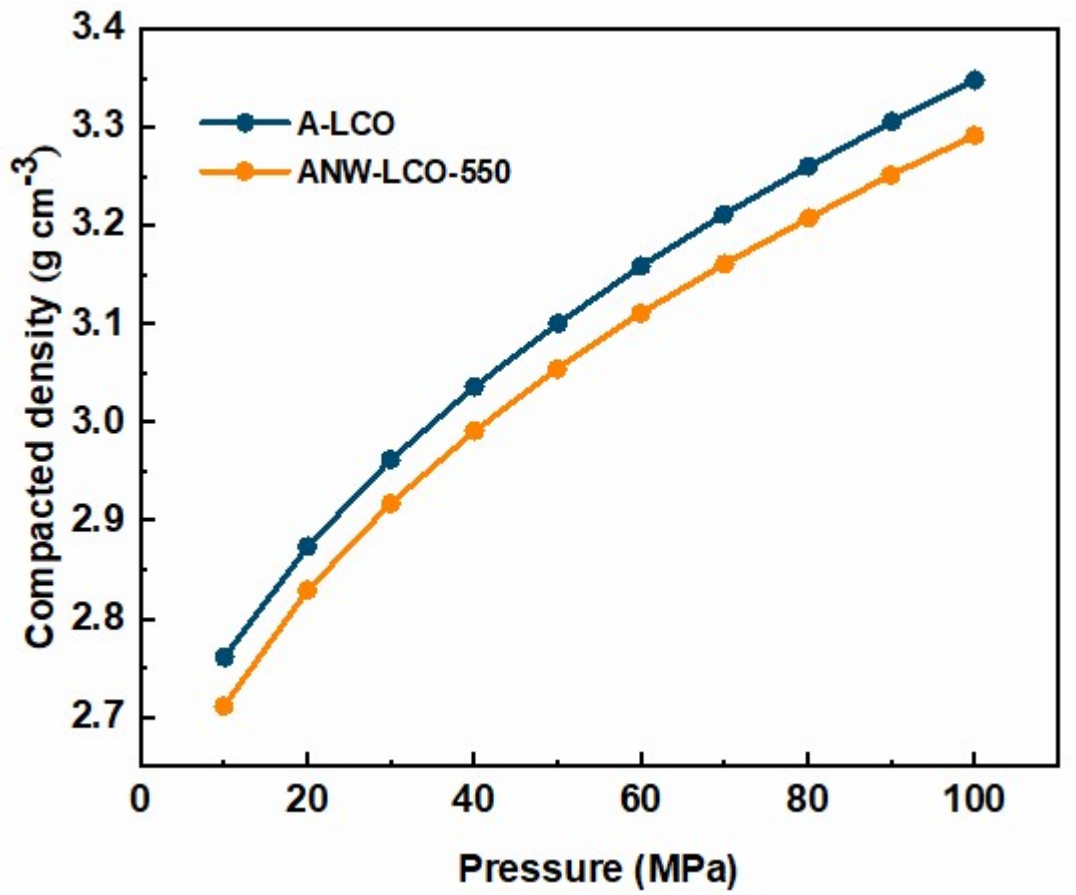


**Figure S16.** The compacted density of A-LCO and ANW-LCO-550.

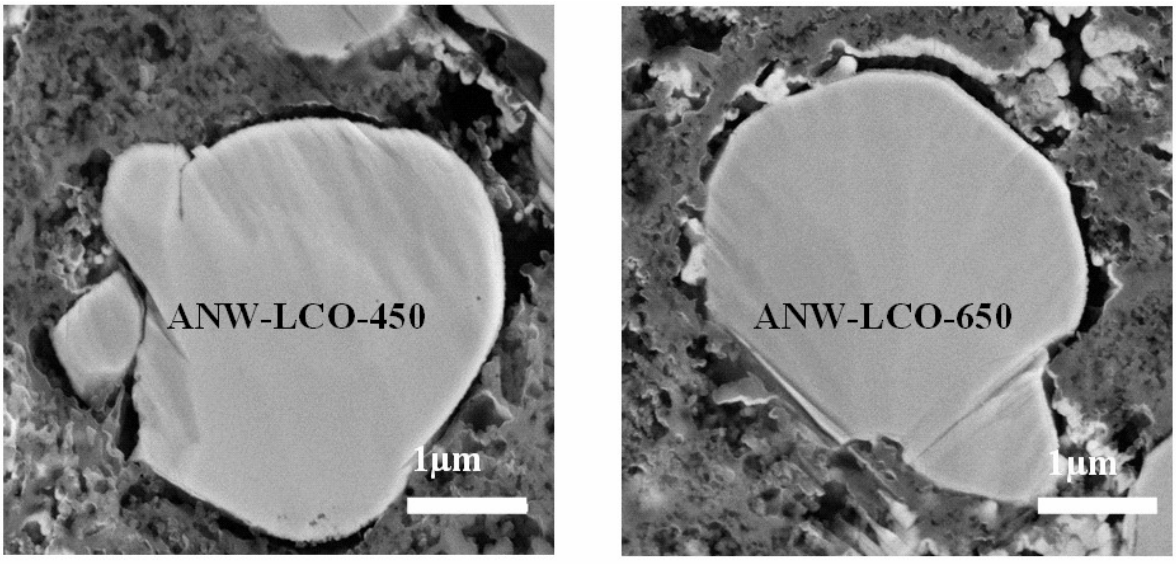


**Figure S17.** SEM images of the cross-section after 100 cycles of ANW-LCO-450, and ANW-LCO-650, scale bar: 1μm.

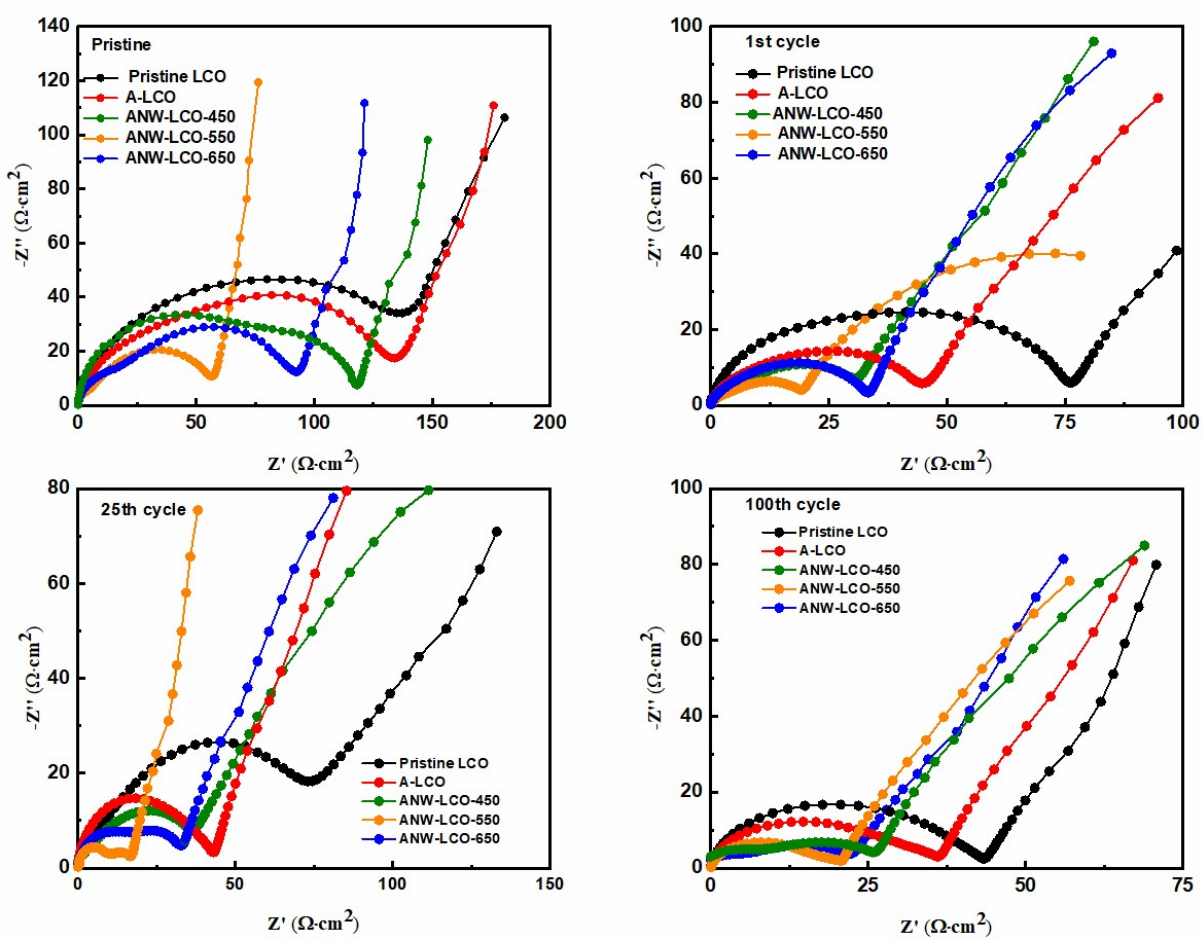


**Figure S18.** Electrochemical impedance spectra of cells with Pristine LCO, A-LCO, ANW-LCO-450, ANW-LCO-550, and ANW-LCO-650 **a.** before cycle, **b.** after 1st cycle, **c.** after 25th cycle, and **d.** after 100th cycle.

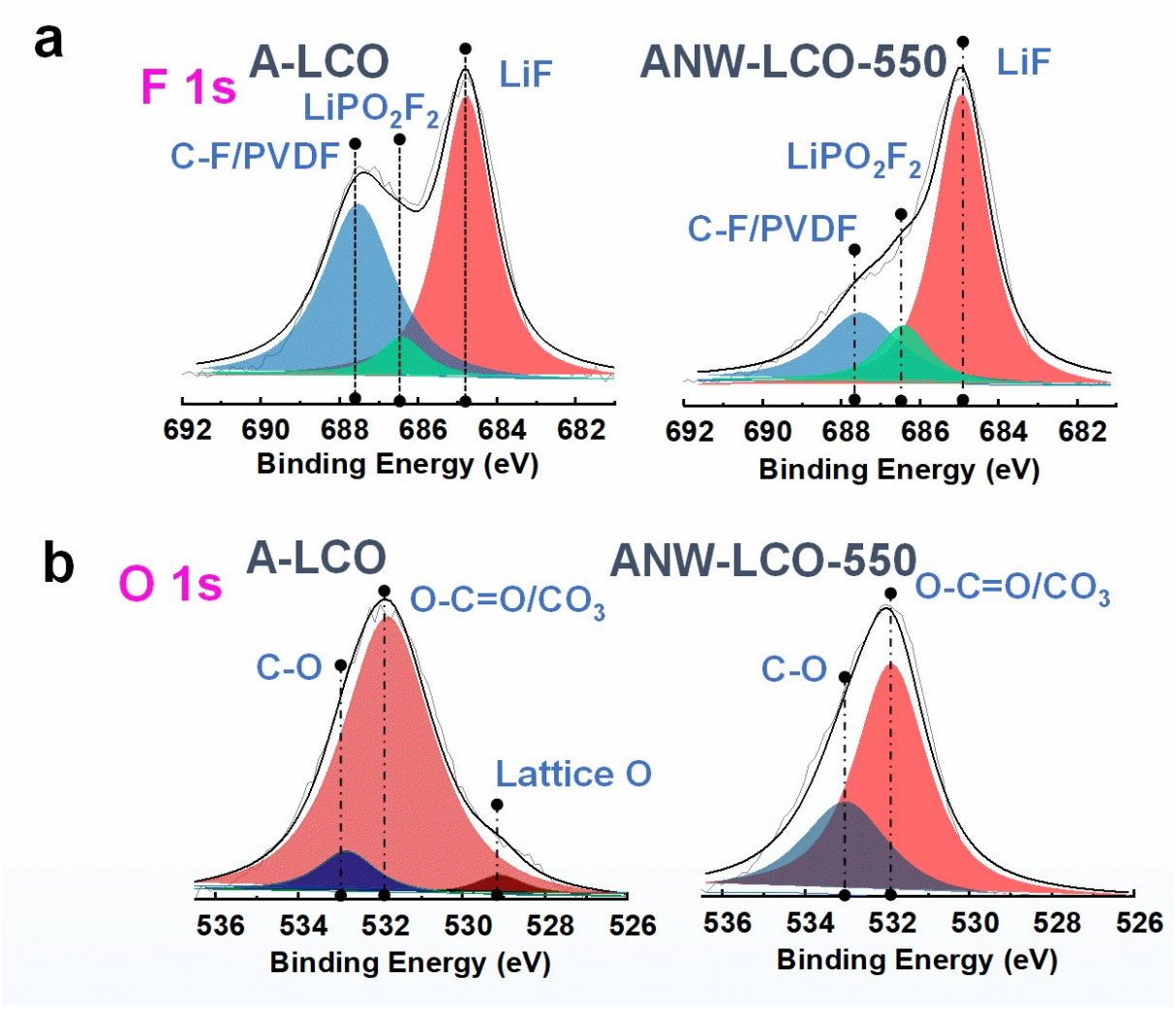


**Figure S19.** a−b) F1s and O 1s XPS spectra of the cycled cathode.

Reference

1 a) J. P. Perdew, K. Burke, M. Ernzerhof, *Phys Rev Lett.* **1996**, 77, 3865; b) B. Hammer, L. B. Hansen, J. K. Nørskov, *Phys. Rev.* B **1999**, 59, 7413; c) P. E. Blöchl, *Phys. Rev.* B **1994**, 50, 17953; d) G. Kresse, D. Joubert, *Phys. Rev.* B **1999**, 59, 1758.

2 H. J. Monkhorst, J. D. Pack, *Phys. Rev.* B **1976**, 13, 5188.

3 a) G. Henkelman, H. Jonsson, *J. Chem. Phys.* **2000**, 113 (22), 9978. b) G. Henkelman, B. P. Uberuaga, H., A Jónsson, *J. Chem. Phys.* **2000**, 113 (22), 9901. c) D. Sheppard, G. Henkelman, *J. Comput. Chem.* **2011**, 32 (8), 1769.